Electronic Supplementary Information (ESI) for

Kinetic and Spectroscopic Insights into the Behaviour of Cu Active Site for NH_3-SCR over Zeolites with Several Topologies

Yusuke Ohata,[a] Hiroe Kubota,[b] Takashi Toyao,[b, c] Ken-ichi Shimizu,[b, c]

Takeshi Ohnishi,[a] Takahiko Moteki [a, c] and Masaru Ogura*[a, c]

a. Institute of Industrial Science, The University of Tokyo, Komaba, Meguro, Tokyo 153-8505, Japan.

E-mail: oguram@iis.u-tokyo.ac.jp

b. Institute for Catalysis, Hokkaido University, N-21, W-10, Sapporo 001-0021, Japan.

c. Elements Strategy Initiative for Catalysts and Batteries, Kyoto University, Katsura, Kyoto 615-8520, Japan

1. Ion-exchange properties of CHA zeolites

In this work, sodium-form zeolites were ion-exchanged in aqueous solution of copper acetate in order to prepare Cu ion-exchanged zeolite catalysts. It is often the case that Cu ion-exchanged zeolites for NH_3-SCR is prepared from Cu ion-exchange of its proton-form zeolites in aqueous solutions of copper nitrate.[S1] However, recent studies on CHA zeolites have shown that the sodium co-cation is more preferable than proton co-cation from the viewpoints of reaction rate at lower reaction temperatures and hydrothermal stability.[S2–4] The copper acetate solution (pH ≈ 6) applied in this study showed weaker acidity than copper nitrate solution (pH ≈ 5) and then undesirable sodium to proton ion-exchange during ion-exchange process can be suppressed. The Cu ion-exchange using the sodium-form zeolites and copper acetate solution for preparation has been adopted onto stoichiometry controlled Cu ion-exchange of zeolites until excessive region to utilize for NO direct decomposition.[S5] Zeolite MOR, MFI, and *BEA were supplied in a sodium form. The detail of Cu ion-exchange of the MOR, MFI, and *BEA zeolites has been reported in the previous report.[S6] The detail of Cu ion-exchange of the samples newly prepared for this work and not included in the previous report were shown in Table S1. CHA zeolites were supplied in a Na/H form (Si/Al = 9) and a NH_4 form (Si/Al = 6.9). Then, they were ion-exchanged to sodium form, and Cu zeolite catalysts were prepared by the following Cu ion-exchange. By the sodium ion-exchange, it was difficult to obtain the fully sodium form with Na/Al = 1. As the results of sodium ion-exchange, CHA zeolites with Si/Al = 9 and Si/Al = 6.9, Na/Al = 0.56 and Na/Al = 0.7 samples were obtained, respectively. It is suggested that the 8MR window of CHA cage is too small to defuse the hydrated sodium cation, or there exist specific Al sites that have small contribution in the ion-exchange process.

Figure S1a shows the profile for sodium to copper ion-exchange. Figure S1b shows the correlation between (2 Cu^{2+} + Na^+)/Al and Cu ion-exchange level. The value of (2 Cu^{2+} + Na^+)/Al is an indicator of stoichiometry for sodium to copper ion-exchange. As shown in Figure S1b, the values of (2 Cu^{2+} + Na^+)/Al are almost constant for CHA zeolite with Si/Al = 6.9. This result suggests that a sodium to copper stoichiometric ion-exchange over this zeolite takes place in the process, and the ion-exchange sites available for the metal cation ion-exchange are around 70 % to the total Al content in this CHA zeolite. On the other hand, for CHA zeolite with Si/Al = 9, the values of (2 Cu + Na)/Al increased gradually with the increase in Cu ion-exchange level (Figure S1b). This result suggests that sodium to copper ion-exchange over this zeolite is not such a stoichiometric process, and indicates that CuOx species with extraframework oxygen might form at higher ion-exchange level region.

2. ^{29}Si MAS NMR spectra of the Model Zeolites

Figures S2a and S2b show ^{29}Si DD and CP MAS NMR spectra of the sodium-formed zeolites used as the parent zeolites in this work, respectively. Table S2 shows the results of the peak fitting of the ^{29}Si DD MAS NMR spectra. In the ^{29}Si DD MAS NMR spectra of the zeolites, a large fraction of the peak assignable to the Q^4(1Al) species around –105 ppm was observed, and small fractions assignable to the Q^4(2Al) around –100 ppm were observed for all zeolites, even in the *BEA or CHA zeolites with high Al contents. It is shown from the

results that the Al atoms contained in the zeolite frameworks are highly delocalized. In the ^{29}Si CP MAS NMR spectra on the zeolites, the Q^3 and Q^2 peaks were hardly observed. These results suggest that a defect site such as the Si–OH groups hardly exists. It is shown by the ^{29}Si MAS NMR spectra that the model zeolites selected in this work hold a relatively delocalized Al site in the framework with high crystallinity.

3. Effect of Zeolite Topology on Reaction Rate for NH_3-SCR at 473 K – MOR and CHA Zeolites with a Similar Si/Al Ratio

Figure S3 shows the reaction rate per Cu for NH_3-SCR at 473 K over the Cu ion-exchanged MOR and CHA zeolites with similar Si/Al ratio plotted as functions of the Cu loading for each zeolite. As shown in the Figure S3, there are obvious differences on the reaction rate per Cu over whole Cu content region and the behavior along with Cu content. The reaction rates per Cu over MOR zeolites were low compared to the CHA zeolite over whole Cu loading region. Moreover, the reaction rates per Cu over MOR zeolite were irrespectively to the Cu loading while those over CHA zeolites were almost in proportion to the Cu content.

The difference in the behavior of reaction rate per Cu along with Cu content over CHA and MOR zeolites can be explained by mobility of Cu^+ coordinated by NH_3 ligands, or the amount of Cu ion that can be reducible by NO + NH_3, according to the following mechanism for NH_3-SCR around 473 K. It is suggested that NH_3-SCR over Cu-CHA zeolites proceeds through the redox between Cu^+ and Cu^{2+}. Reduction of Cu^{2+} proceeds by reaction with NO + NH_3 and oxidation of Cu^+ mainly by O_2. The formed Cu^+ during NH_3-SCR is thought to be mobile in the zeolite micropore coordinated by NH_3, and the oxidation undergoes through O-bridged dimetric intermediates.[S7–9] In the case of CHA zeolites, it have been suggested that the average distance among Cu ions decreases and the rate-determining $Cu^+ \rightarrow Cu^{2+}$ oxidation step are promoted with the increase of the Cu ion space density. [S8, 9] The trend of the reaction rate per Cu for the CHA zeolites in this work shows good agreement to the above description.

It has been reported in the comparative study among the CHA, AEI, and RTH zeolites[S10] that the reaction rate over RTH zeolite is smaller than those over two other zeolites. This phenomenon is explained by the existence of a constrained and asymmetric 8 MR window (0.56 nm × 0.25 nm) in RTH framework and by the limitation of the pore connectivity. A MOR zeolites with 12 MR channel has a constrained and asymmetric 8 MR window (0.57 nm × 0.26 nm)[S11], and is expected to work as a one-dimensional pore system for NH_3-SCR similar to RTH zeolite with 8 MR main channel. When the discussion is limited on the value of the reaction rate, the low reaction rate per Cu over MOR zeolites compared with the CHA zeolite observed in this work has good agreement with the above explanation. However, it is reported in the other report[S12] that turnover frequency (TOF) increases along with Cu content even over RTH zeolite with a low dimension channel system. Therefore, it is difficult to explain the behavior along with Cu loading over MOR zeolite only by one dimension channel system, and other factors are needed that inhibit the increase of reaction rate for NH_3-SCR along with the increase of Cu loading (= Cu ion space density) in MOR zeolite.

The transient response in the feed switch from dried N_2 to 500 ppm NO + 500 ppm NH_3 in dried N_2 at

473 K over 1.8 wt.% Cu loaded Cu-zeolites (36 % ion-exchange level of Cu^{2+}) was conducted. In this process, the following stoichiometric reaction is assumed to take place:

$$Cu^{2+} + NO + 4\ NH_3 \rightarrow N_2 + [H_3N–Cu^{+}–NH_3]^{+} + NH_4^{+} + H_2O \quad (1)$$

Therefore, the amount of Cu ion contributed to the NH_3-SCR can be estimated from the consumed amount of NO in this process, and the coordination state of Cu^{+}, which is thought to be mobile during the NH_3-SCR at 473 K, can be estimated from the consumed amount of NH_3 in this process. In summary, this measurement was conducted to estimate the difference in amount of Cu ion contributed to the NH_3-SCR and the mobility of Cu^{+} on different zeolites. As the background, the profiles of the same transient response over parent sodium-form zeolites were used. Because of the preparation conditions described above, it was confirmed that the Cu-zeolites in this work have a small amount of H^{+} as the counter cation. Moreover, the transient response over parent zeolites at 473 K showed that they have little NH_3 adsorption capacity and almost all of adsorbed NH_3 are reversible. It was confirmed that equilibrated NH_3 concentration of breakthrough curve and the elution curve over the Cu ion-exchanged zeolites were almost the same as those over parent sodium-form zeolite. Therefore, it can be thought that quantification of the amount of consumed NH_3 in the process related to the Cu ion can be estimated by this method.

Table S3 shows the amount of Cu contained in the zeolites obtained by ICP-AES measurement, consumed NO, and consumed NH_3 in the transient reaction over 1.8 % Cu loaded CHA and MOR zeolites. In the case of MOR zeolite, consumed NO was almost equal to the amount of Cu, and consumed NH_3 was 2.5 times larger than NO. In the case of CHA zeolite, consumed NO was slight smaller than Cu, and consumed NH_3 was 2.3 times larger than NO. It is shown by the consumed amount of NO that the almost all of contained Cu on both zeolites is isolated species that can be reduced by NO + NH_3. Moreover, it is shown by the calculated molar ratio of NH_3/NO that the state of reduced Cu^{+} is almost equal on both zeolites. The observed NH_3/NO molar ratio is smaller than that predicted from the Eq. (1). This result can be explained by the contribution of the following two equations:

$$Cu^{2+} + NO + 3\ NH_3 \rightarrow N_2 + [H_3N–Cu^{+}–NH_3]^{+} + H^{+} + H_2O \quad (2)$$

$$Cu^{2+} + NO + 2\ NH_3 \rightarrow N_2 + [H_3N–Cu^{+}–OH] + 2\ H^{+} \quad (3)$$

In summery, it is suggested that the amount of isolated Cu ion and the state of Cu^{+} complex during the NH_3-SCR at 473 K is similar on MOR and CHA zeolites from the transient response measurement. Nevertheless, it was observed that the reaction rate per Cu for the MOR zeolite is far smaller than the reaction rate per Cu for the CHA zeolites over whole Cu loading region. Moreover, the reaction rate per Cu for the MOR zeolites was almost constant with increase of the Cu loading while reaction rate per Cu for the CHA zeolites increased with Cu loading. In summary, it is suggested that there are some factors that inhibit increase in the reaction rate along with increase in Cu content (= increase in the density of Cu ion) on the MOR zeolites, and the factor is not due to the accommodation property of isolated Cu ion or the difference in the state of Cu^{+}, which is thought to be the complex with high mobility.

4. Effect of Si/Al Ratio on Reaction Rate for NH_3-SCR at 473 K – CHA, MFI, and *BEA Case

Figure S4 shows the correlation between the reaction rate for NH_3-SCR at 473 K and Cu loading over Cu ion-exchanged CHA, *BEA, and MFI zeolites with various Si/Al ratio. Note that it is revealed by ICP-AES measurement that Si/Al ratio is 17 after the sodium ion-exchange of *BEA zeolite with Si/Al =14. As shown in Figure S4, the trend was observed that reaction rates per Cu over lower Si/Al ratio zeolites were larger than those over higher Si/Al ratio ones in the whole Cu loading. Note that reaction rate per Cu on FAU zeolite with Si/Al = 2.8 was far lower than those of any other zeolites with the same Cu loading. Then, it is shown that the high reaction rate for NH_3-SCR is not explained only by the low Si/Al ratio of zeolites. Over all of those zeolites, the reaction rates per Cu increased linearly with increase of the ion-exchange level of Cu. Interestingly, the behavior of the rates per Cu over the MFI and *BEA zeolites as the function of the Cu content were almost parallel to each other. Moreover, the effect of Si/Al ratio of parent zeolites was mainly observed in the extrapolation value at 0 on the plots of each zeolite. On the other hand, the effect of Si/Al ratio of parent zeolites were mainly observed in the slope of lines in the case for the CHA zeolites.

Figure S5 shows the relationships between Na ion-exchange level and Cu ion-exchange level of the *BEA and MFI zeolites. The stoichiometric ion-exchange from Na to Cu was observed in the profiles shown in Figure S5, suggesting that almost all Cu is ionic. Moreover, both zeolites have a three-dimensional channel structure and there is no restriction on the pore connectivity. Therefore, it is difficult to explain the difference in the extrapolation value at 0 observed on the plots for *BEA and MFI zeolites under the understanding that the rates for NH_3-SCR are determined only by Cu loading or Cu volumetric density[S7, 9] regardless of zeolite structures. However, it can be estimated that zeolites without enough Al content in the framework have some inhabitation effect on the reaction compared in the zeolites with the same topology, maybe due to the localized cation exchange site distribution.

In summary, it is suggested that the model zeolites from which the factors are avoided except zeolite topology that might limit the reaction rate should be selected toward the comparative study on the catalytic activity for NH_3-SCR. In this line of consideration, the “Cation Density per Micropore” was defined.

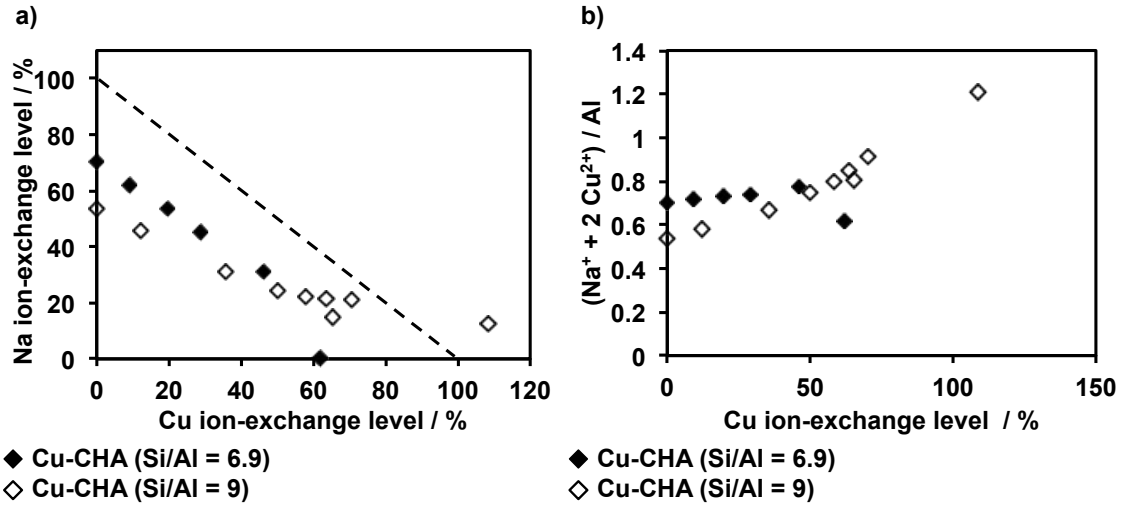

Figure S1. (a) Correlation between the Na ion-exchange level and Cu ion-exchange level, or (b) Cu ion-exchange level and $(Na^+ + 2\ Cu^{2+})/Al$ of the CHA zeolites (Si/Al = 6.9; ◆, Si/Al = 9; ◇). Na ion-exchange level were calculated at Na/Al = 1 as 100 % because the sodium ion is monovalent. Cu ion-exchange level were calculated at Cu/Al = 0.5 as 100 % because the copper ion is divalent.

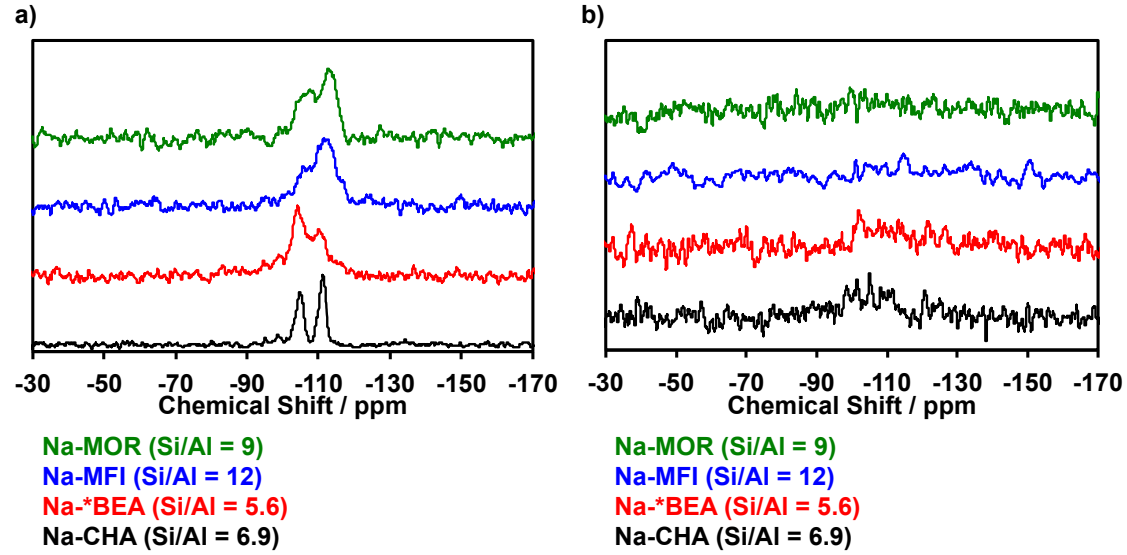

Figure S2. (a) ^{29}Si DD MAS NMR spectra and (b) ^{29}Si CP MAS NMR spectra of the sodium-formed zeolites used as the parent zeolites.

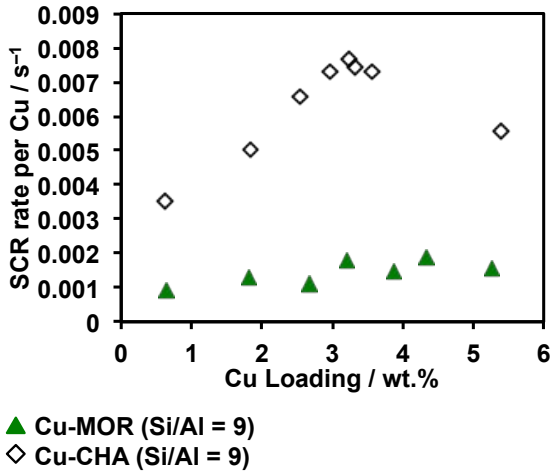

Figure S3. Correlation between the standard NH_3-SCR rate per Cu at 473 K and Cu loading over the MOR (▲) and CHA(◇) zeolites with Si/Al = 9.

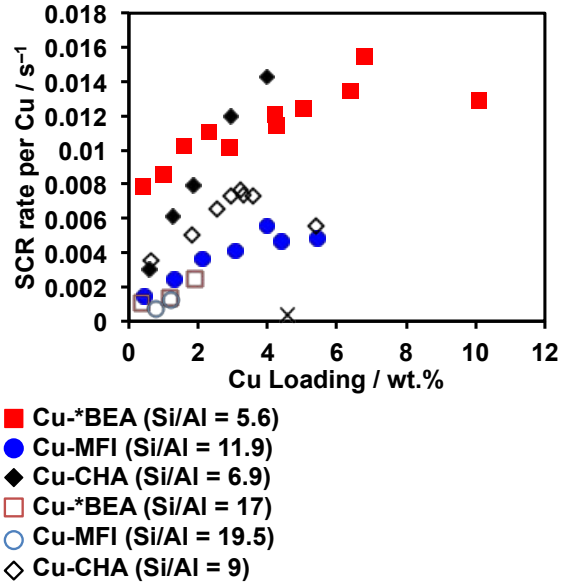

Figure S4. Correlation between the standard NH_3-SCR rate per Cu at 473 K and Cu loading over the MFI (●), *BEA (■), CHA(◆), and FAU(×) zeolites with various Si/Al. The filled symbols show the zeolites with lower Si/Al and the hollow symbols show the zeolites with higher Si/Al.

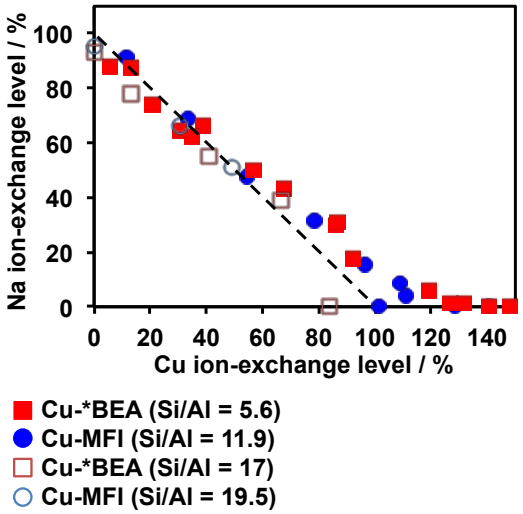

Figure S5. Correlation between the Na ion-exchange level and Cu ion-exchange level of the *BEA (Si/Al = 5.6; ■), *BEA (Si/Al = 17; □), MFI (Si/Al = 11.9; ●), and MFI (Si/Al = 19.5; ○) zeolites. Na ion-exchange level were calculated at Na/Al = 1 as 100 % because the sodium ion is monovalent. Cu ion-exchange level were calculated at Cu/Al = 0.5 as 100 % because the copper ion is divalent.

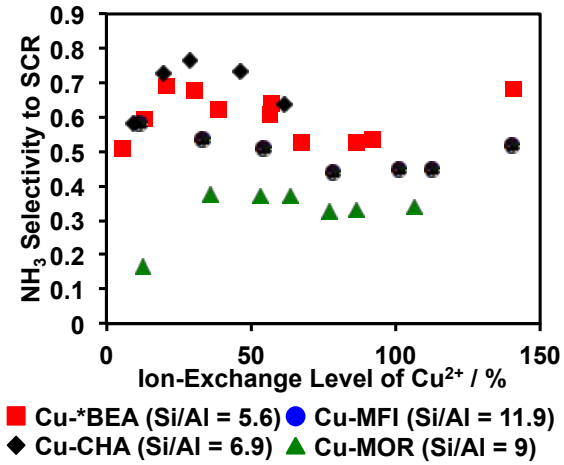

Figure S6. Correlation between the NH_3 selectivity to SCR in the NH_3-SCR at 873 K and Cu ion-exchange level over the MOR (▲), MFI (●), *BEA (■), and CHA(◆) zeolites.

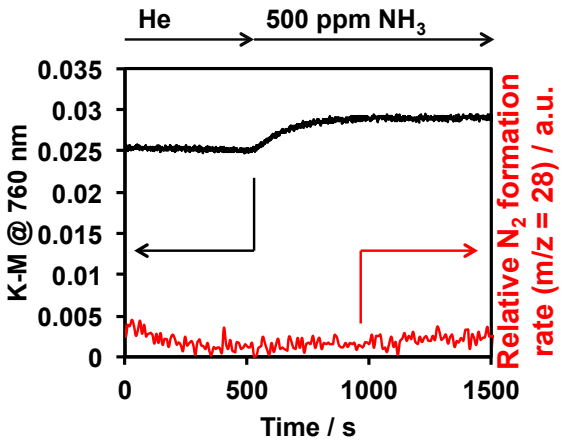

Figure S7. Time-resolved UV-Vis profiles for the KM at 760 nm (d-d transition band of Cu^{2+}) and MS intensity of *m/z* = 28 (N_2) of Cu-*BEA (21 % Cu ion-exchange level) in the transition response switching to 500 ppm NH_3 flow.

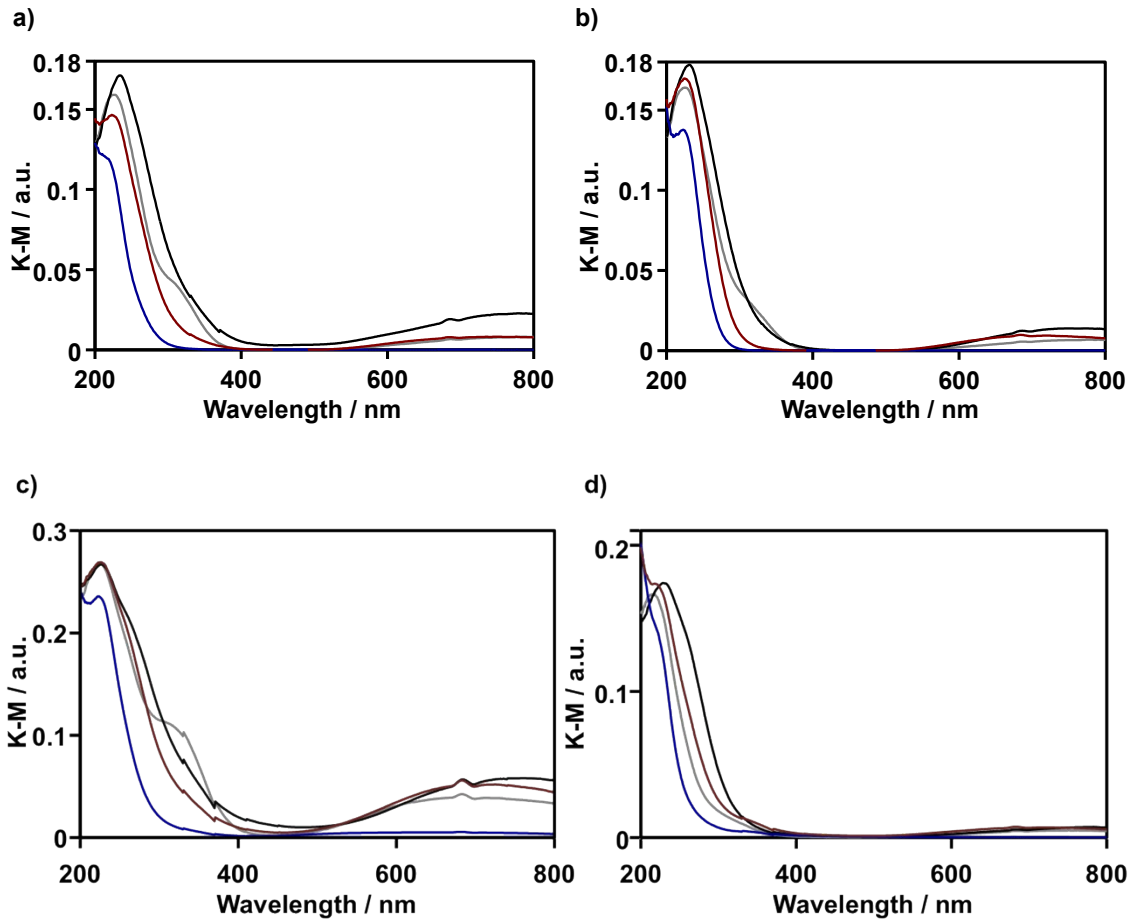

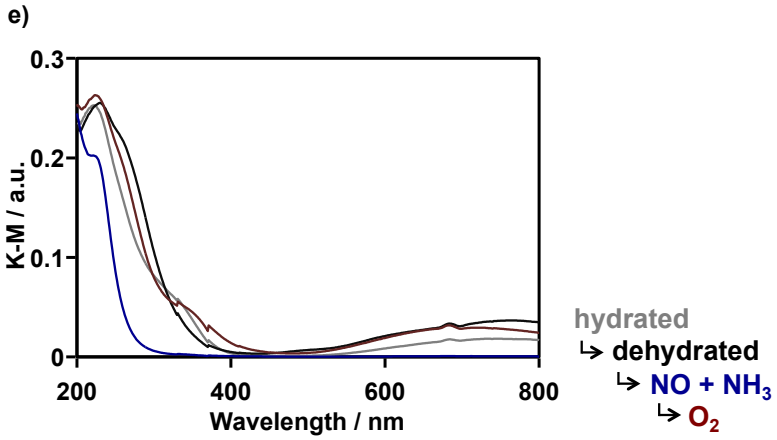

Figure S8. *In-situ* UV-Vis spectra of (a) Cu-MOR (36 % Cu ion-exchange level), (b) Cu-MFI (33 % Cu ion-exchange level), (c) Cu-MFI (101 % Cu ion-exchange level), (d) Cu-CHA (9.3 % Cu ion-exchange level), (e) Cu-CHA (29 % Cu ion-exchange level) during Scheme 2. Gray, black, blue, and blown line show the spectrum in hydrated condition under He (100 cm^3 min^{-1}) flow at room temperature, after dehydrated by 5 % O_2/He at 873 K under He (100 cm^3 min^{-1}) flow, after reduction by 500 ppm NO + 500 ppm NH_3/He (100 cm^3 min^{-1}) flow, and after reoxidation by 5 % O_2/He (100 cm^3 min^{-1}) flow, respectively. In the measurement, temperature was kept at 473 K other than the hydrated condition, and the flow gas was same as the treatment condition unless otherwise noted.

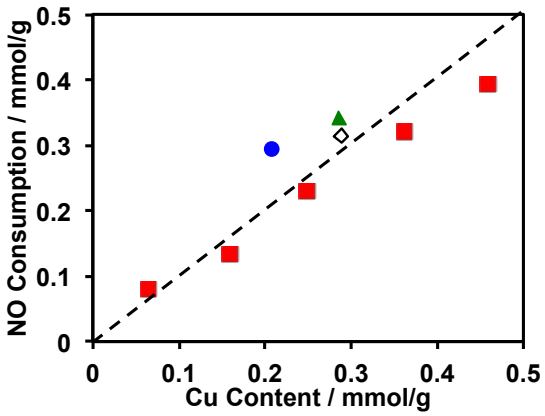

Figure S9. Relationship between the ICP-AES based Cu content of the Cu-zeolites and the amount of Cu^{2+} estimated by consumed amount of NO during the transient response at 473 K according to **Scheme B**.

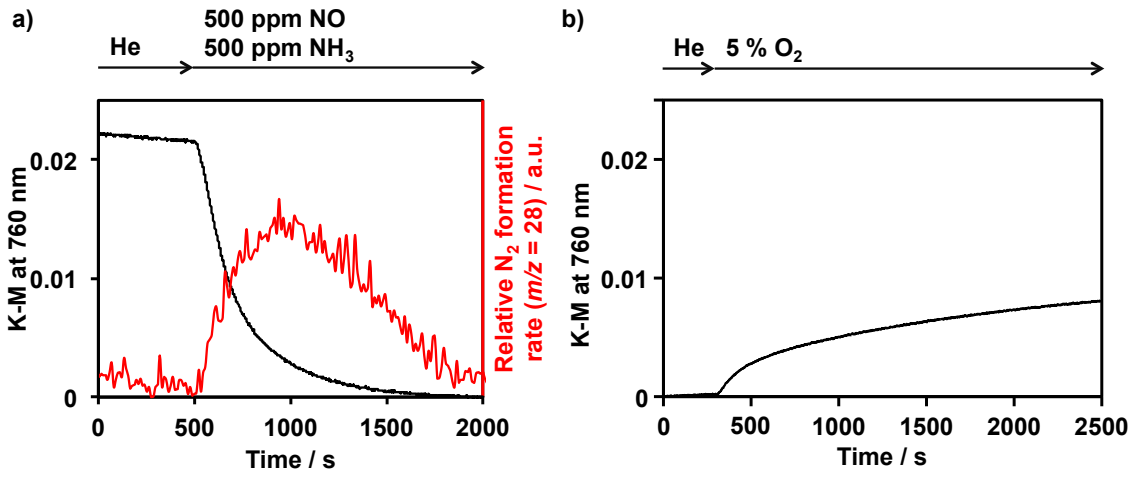

Figure S10. Time-resolved UV-Vis profiles for the KM at 760 nm (d-d transition band of Cu^{2+}) and MS intensity of *m/z* = 28 (N_2) of Cu-MOR (36 % Cu ion-exchange level) in the transition response switching to (a) 500 ppm NH_3 + 500 ppm NO flow and (b) 5 % O_2 flow at 473 K.

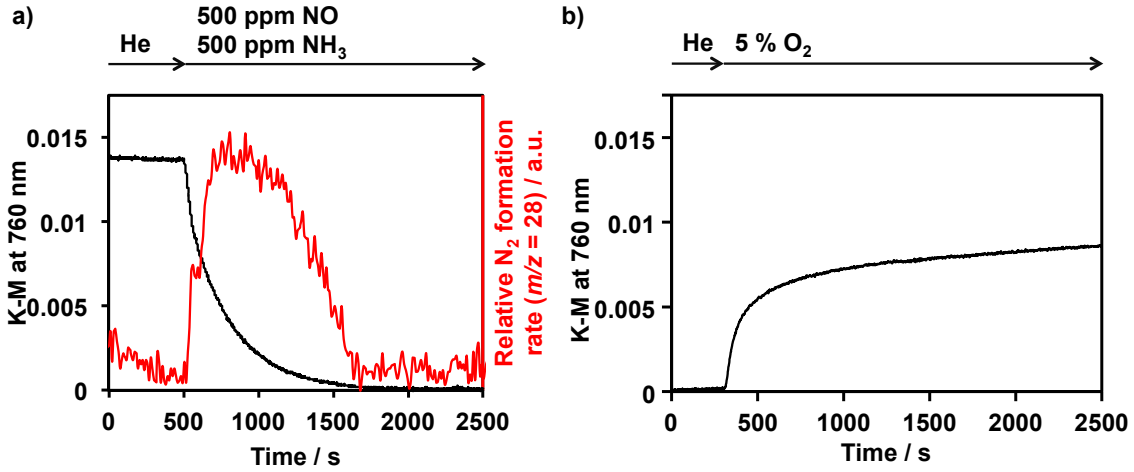

Figure S11. Time-resolved UV-Vis profiles for the KM at 760 nm (d-d transition band of Cu^{2+}) and MS intensity of *m/z* = 28 (N_2) of Cu-MFI (33 % Cu ion-exchange level) in the transition response switching to (a) 500 ppm NH_3 + 500 ppm NO flow and (b) 5 % O_2 flow at 473 K.

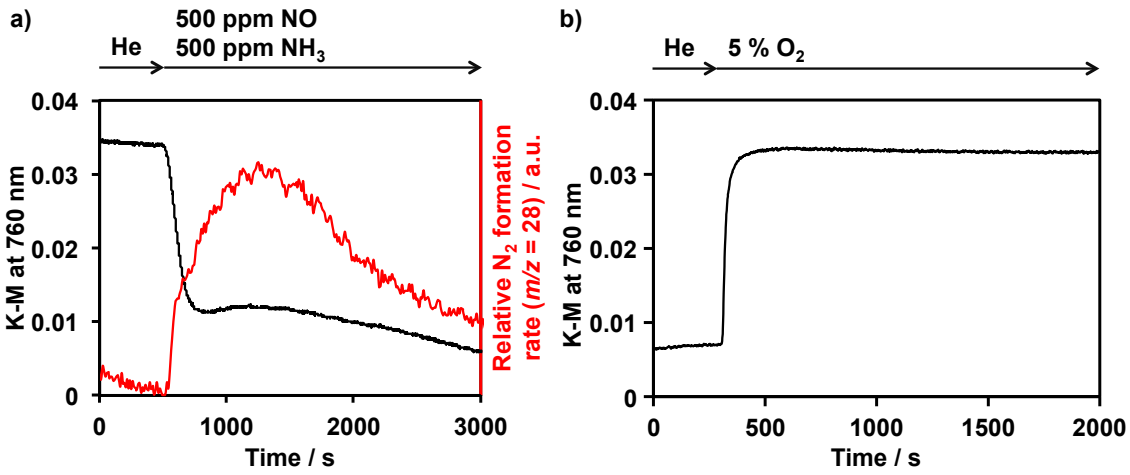

Figure S12. Time-resolved UV-Vis profiles for the KM at 760 nm (d-d transition band of Cu^{2+}) and MS intensity of *m/z* = 28 (N_2) of Cu-*BEA (39 % Cu ion-exchange level) in the transition response switching to (a) 500 ppm NH_3 + 500 ppm NO flow and (b) 5 % O_2 flow at 473 K.

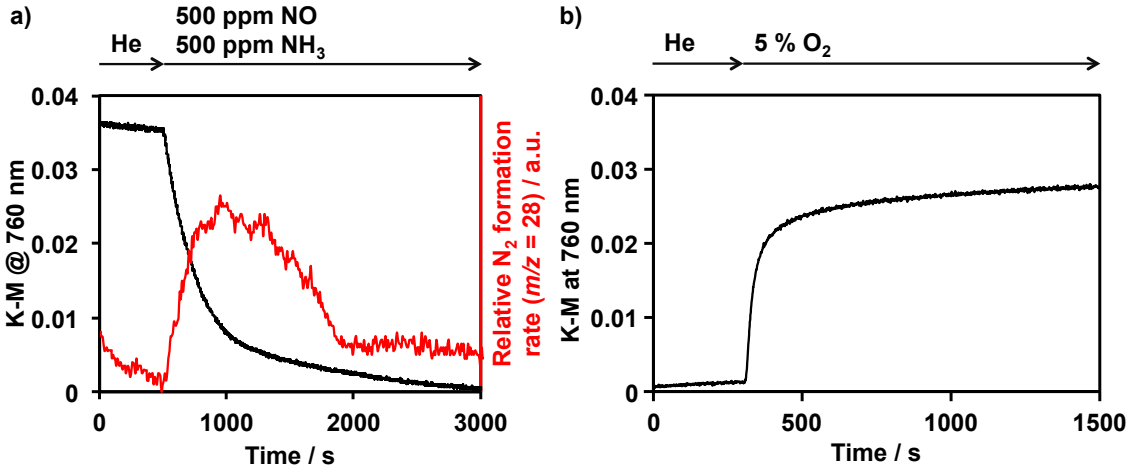

Figure S13. Time-resolved UV-Vis profiles for the KM at 760 nm (d-d transition band of Cu^{2+}) and MS intensity of *m/z* = 28 (N_2) of Cu-CHA (29 % Cu ion-exchange level) in the transition response switching to (a) 500 ppm NH_3 + 500 ppm NO flow and (b) 5 % O_2 flow at 473 K.

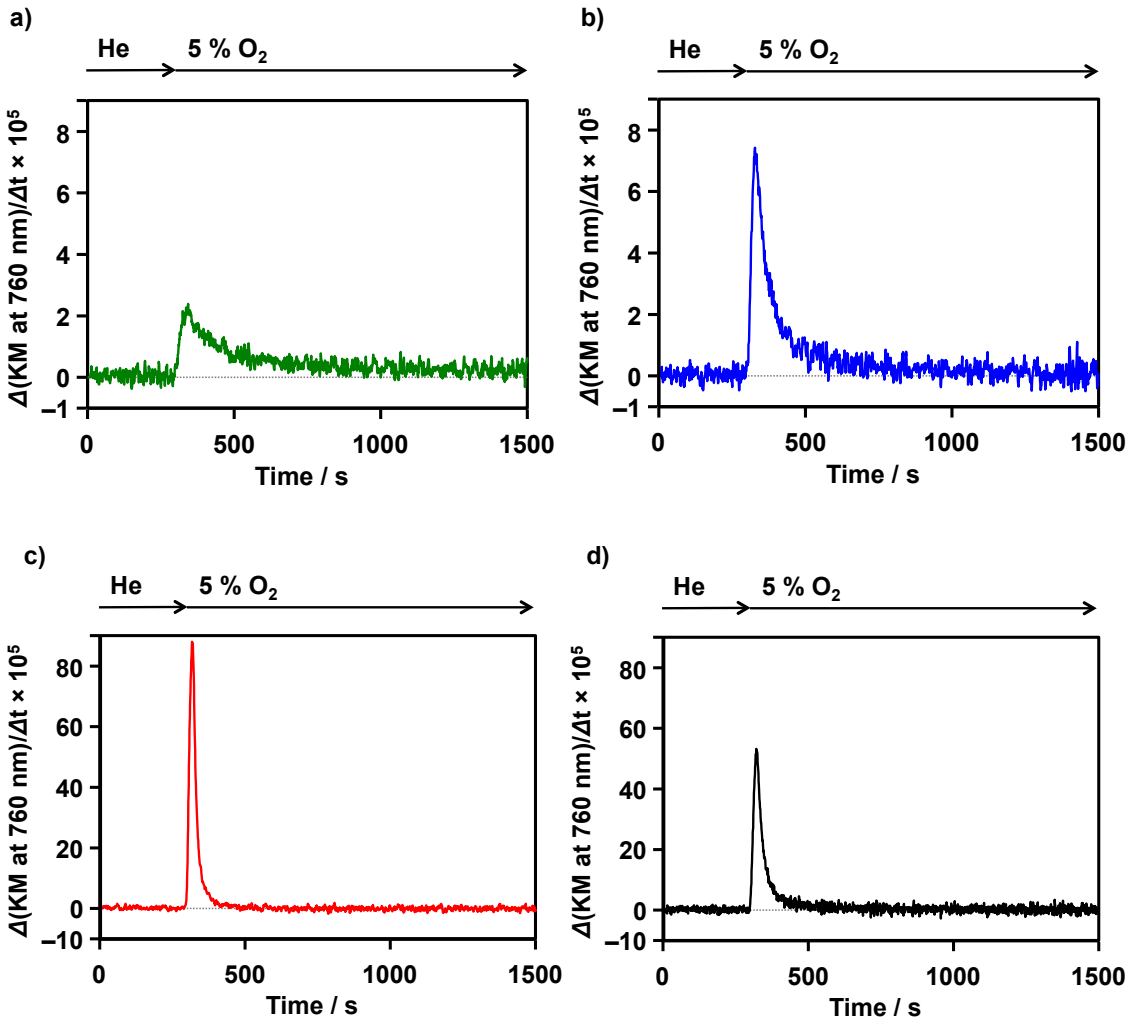

Figure S14. The time derivative of time-resolved UV-Vis profiles for the KM at 760 nm (d-d transition band of Cu^{2+}) of (a) Cu-MOR (36 % Cu ion-exchange level), (b) Cu-MFI (33 % Cu ion-exchange level), (c) Cu-*BEA (36 % Cu ion-exchange level), and (d) Cu-CHA (29 % Cu ion-exchange level)in the transition response switching to 5 % O_2 flow at 473 K.

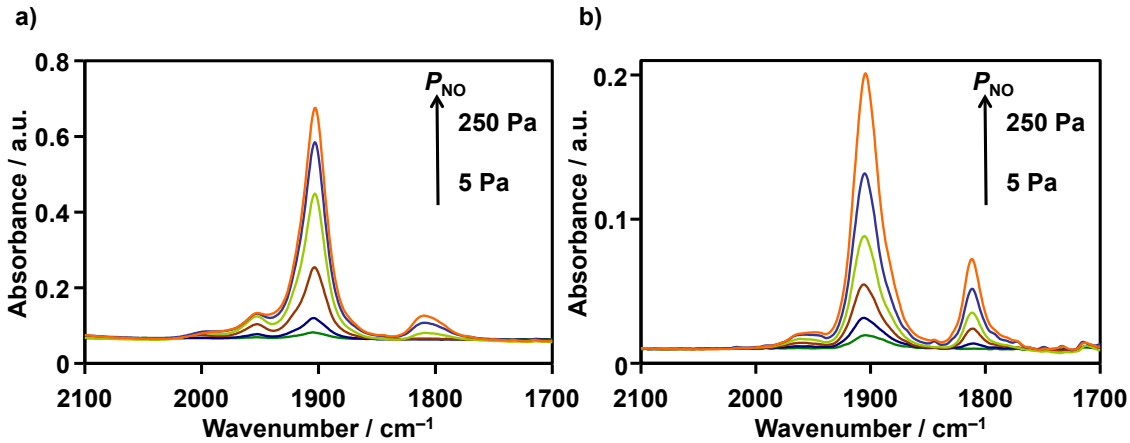

Figure S15. IR spectra of NO adsorbed on the (a) Cu-MOR (36 % Cu ion-exchange level) and (b) Cu-MFI (33 % Cu ion-exchange level) zeolites at room temperature (ca. 25 °C) after 15 kPa O_2 treatment at 773 K.

Table S1. Copper ion-exchange condition and ion-exchange level of the obtained Cu ion-exchanged zeolite samples prepared in this study.

Entry.	Parent	Molarity / mmol L^{-1}	Repeat times	Cu Ion-Exchange Level[(a)] / %	Na Ion-Exchange Level[(b)] / %
B11	Na-*BEA (Si/Al = 5.6)	0.91	1	5.3	88
B12		2.0	1	13	88
B13		3.6	1	21	74
B14		5.4	1	30	65
Z11	Na-MFI (Si/Al = 12)	0.94	1	12	91
Z12		10	2	101	0
M11	Na-MOR (Si/Al = 9)	1.2	1	13	90
C1	Na-CHA (Si/Al = 6.9)	1.5	1	9.3	62
C2		3.0	1	20	53
C3		4.5	1	29	45
C4		7.5	1	46	31
C5		12.1	1	62	0
C901	Na-CHA (Si/Al = 9)	1.3	1	12	46
C902		4.0	1	36	31
C903		6.7	1	50	25
C904		10.7	1	58	22
C905		15	1	64	21
C906		30	1	70	21
C907		10	3	65	15
C908		30	3	109	12
B171	Na-*BEA (Si/Al = 17)	0.81	1	13	78
B172		2.4	1	41	55
B173		4.1	1	66	39
Z191	Na-MFI (Si/Al = 19.5)	1.8	1	31	66
Z192		3.0	1	49	51
F1	Na-FAU (Si/Al = 2.8)	9.0	1	36	61

(a) Cu Ion-exchange level / % = (amount of Cu)/(amount of Al) × 200

(b) Na Ion-exchange level / % = (amount of Na)/(amount of Al) × 100

Table S2. Ratio of the each Si species obtained by the deconvolution of ^{29}Si DDMAS NMR spectra of zeolites.

Zeolite	Peak / ppm	Area ratio / %	Assignment
Na-MOR (Si/Al = 9)	–104.3	14.3	Q^4(1Al)
	–107.6	38.4	Q^4(1Al)
	–113.2	47.3	Q^4(0Al)
Na-MFI (Si/Al = 12)	–105.7	24.8	Q^4(1Al)
	–112.1	75.2	Q^4(0Al)
Na-*BEA (Si/Al = 5.6)	–85.7	6.3	SiOH
	–94.8	4.6	SiOH
	–98.7	5.2	Q^4(2Al)
	–104.3	45.4	Q^4(1Al)
	–110.2	35.5	Q^4(0Al)
	–115.9	3.1	Q^4(0Al)
Na-CHA (Si/Al = 6.9)	–98.9	8.5	Q^4(2Al)
	–103.0	5.0	Q^4(1Al)
	–104.9	37.7	Q^4(1Al)
	–109.8	9.5	Q^4(0Al)
	–111.3	39.3	Q^4(0Al)

Table S3. Cu contained amount and consumed amount of reactants in the transient reaction at 473 K.

Entry.	Cu content / mmol/g	NO consumption / mmol/g	NH_3 consumption / mmol/g	NH_3/NO
C902	0.29	0.25	0.56	2.3
M2	0.29	0.30	0.76	2.5

Table S4. Area ratio of observed adspecies, Area ratio between the band at 1904 cm^{-1} and those at 1895 cm^{-1}, and the position of peak maximums of d-d transition bands observed in UV-Vis spectra over zeolites with different topologies.

Zeolite	Peak / cm^{-1}	Area ratio / %	$\frac{A\ (1895\ cm^{-1})}{A\ (1904\ cm^{-1})}$	d-d transition band in UV-Vis spectra
Na-MOR (Si/Al = 9)	1953	7.66	0	777
	1919	7.74		
	1903	84.6		
Na-MFI (Si/Al = 12)	1915	6.09	0.36	753
	1904	69.1		775
	1886	24.8		
Na-*BEA (Si/Al = 5.6)	1965	6.56	3.29	745
	1929	11.9		
	1905	19.0		
	1895	62.5		
Na-CHA (Si/Al = 6.9)	1947	8.95	2.69	762
	1931	3.33		
	1923	18.6		
	1912	15.0		
	1903	14.7		
	1891	39.4		

References

[S1] J. H. Kwak, R. G. Tonkyn, D. H. Kim, J. Szanyi and C. H. F. Peden, *J. Catal.,* 2010, **275**, 187.

[S2] F. Gao, Y. Wang, N. M. Washton, M. Kollaŕ, J. Szanyi and C. H. F. Peden, *ACS Catal.,* 2015, **5**, 6780.

[S3] Y. Cui, Y. Wang, D. Mei, E. D. Walter, N. M. Washton, J. D. Holladay, Y. Wang, J. Szanyi, C. H. F. Peden and F. Gao, *J. Catal.,* 2019, **378**, 363.

[S4] Y. Cui, Y. Wang, E. D. Walter, J. Szanyi, Y. Wang and F. Gao, *Catal. Today,* 2020, **339**, 233.

[S5] H. Yahiro and M. Iwamoto, *How to Prepare Heterogeneous and Homogeneous Catalysts,* ed. M. Iwamoto, NTS, Tokyo, 2011, Chap. 3, 246.

[S6] Y. Ohata, T. Nishitoba, T. Yokoi, T. Moteki and M. Ogura, *Bull. Chem. Soc. Jpn.,* 2019, **92**, 1935.

[S7] C. Paolucci, A. A. Parekh, I. Khurana, J. R. Di Iorio, H. Li, J. D. A. Caballero, A. J. Shih, T. Anggara, W. N. Delgass, J. T. Miller, F. H. Ribeiro, R. Gounder and W. F. Schneider, *J. Am. Chem. Soc.,* 2016, **138**, 6028.

[S8] F. Gao, D. Mei, Y. Wang, J. Szanyi and C. H. F. Peden, *J. Am. Chem. Soc.,* 2017, **139**, 4935.

[S9] C. Paolucci, I. Khurana, A. A. Parekh, S. Li, A. J. Shih, H. Li, J. R. Di Iorio, J. D. Albarracin-Caballero, A. Yezerets, J. T. Miller, W. N. Delgass, F. H. Ribeiro, W. F. Schneider and R. Gounder, *Science,* 2017, **357**, 898.

[S10] J. D. Albarracin-Caballero, I. Khurana, J. R. Di Iorio, A. J. Shih, J. E. Schmidt, M. Dusselier, M. E. Davis, A. Yezerets, J. T. Miller, F. H. Ribeiro and R. Gounder, *React. Chem. Eng.,* 2017, **2**, 168.

[S11] Database of Zeolite Structures, http://www.iza-structure.org/ databases/.

[S12] Y. Shan, X. Shi, J. Du, Y. Yu and H. He, *Catal. Sci. Technol.,* 2019, **9**, 106.